Crystal Growth and Dissolution of Calcite in the Presence of Fluoride Ions: An Atomic Force Microscopy Study

ARTICLE *in* CRYSTAL GROWTH & DESIGN · JANUARY 2010

Impact Factor: 4.89 · DOI: 10.1021/cg900131g

4 AUTHORS, INCLUDING:

Aikaterini I Vavouraki
University of Patras
13 PUBLICATIONS **105** CITATIONS
SEE PROFILE

Andrew Putnis
University of Münster
128 PUBLICATIONS **2,804** CITATIONS
SEE PROFILE

Petros Koutsoukos
University of Patras
231 PUBLICATIONS **4,905** CITATIONS
SEE PROFILE

DOI: 10.1021/cg900131g

CRYSTAL GROWTH & DESIGN Article
XXXX, Vol. XXX
000–000

Crystal Growth and Dissolution of Calcite in the Presence of Fluoride Ions: An Atomic Force Microscopy Study

Aikaterini I. Vavouraki,*[,§,†,‡] Christine V. Putnis,[§] Andrew Putnis,[§] and Petros G. Koutsoukos[†,‡]

[§]*Institut für Mineralogie, Universität Münster, Corrensstrasse 24, D-48149 Münster, Germany,* [†]*Department of Chemical Engineering, University of Patras, Karatheodori 1, 26500 Rio, Patras, Greece, and* [‡]*Institute of Chemical Engineering & High Temperature Chemical Processes, Stadiou Street, Platani, P.O. Box 1414, GR-26504, Patras, Greece*

Received February 4, 2009; Revised Manuscript Received September 23, 2009

ABSTRACT: Growth and dissolution of calcite $\{10\bar{1}4\}$ surfaces in aqueous solutions in the presence of fluoride ions have been studied by in situ atomic force microscopy (AFM). Supersaturated and undersaturated solutions with respect to calcite were prepared for the growth and dissolution experiments, respectively. The concentration range of solutions containing fluoride ions varied between 0.025 and 50 mM. The crystal growth rates were measured from the step growth of closing of etch pits along the [010] direction as well as the spreading of two-dimensional growth nuclei in the same direction. Dissolution rates were measured from the time-dependent development of the rhombohedral etch pits along both [010] and $[42\bar{1}]$ directions. Low fluoride concentrations ($\leq$0.33 mM) in the supersaturated solutions did not significantly affect the crystal growth rates of calcite. At higher concentrations (up to 5 mM), the growth rate decreased substantially, reaching 50% of the respective rate in the absence of fluoride for the same supersaturation. It is suggested that the fluoride ions acted as inhibitors of calcite crystal growth, possibly through adsorption at the active growth sites. For dissolution experiments, the presence of both low and high fluoride concentrations ($\leq$1.1 mM and up to 50 mM) accelerated the rate of dissolution along the $[42\bar{1}]$ direction up to 70% of the respective rate in pure water. The presence of fluoride changed the morphology of the dissolving rhombohedral etch pits to hexagonal. The morphology patterns of the dissolving calcite surface recorded by AFM imaging in the presence of fluoride ions suggested also that the fluoride ions were adsorbed onto the calcite surface. It seems likely that calcite growth and dissolution from aqueous solutions containing fluoride ions are governed by a complex interaction between the surface characteristics of the calcite crystal as well as changes in solvent structure, surface hydration, and ion solvation induced by the presence of fluoride.

I. Introduction

Precipitation and dissolution of carbonate minerals play a major role in the formation of sediments and sedimentary rocks, as well as during weathering. These processes also play a key role in the design of conservation strategies for historical buildings made of limestone and related materials. Variation of physicochemical parameters (e.g., pH, temperature, fluid flow ionic strength) at the stone−water interface influence precipitation and dissolution mechanisms. The interaction of the solid with foreign substances, such as pollutants or treatment agents may affect the structure of the crystallites of the corresponding materials.[1] The kinetics of growth and dissolution of carbonate mineral crystals has been reported to be dramatically affected by the presence of traces of impurities or additives.[2−4] The growing interest in understanding crystal growth and dissolution of calcite at the molecular level is reflected in the large number of recent publications concerned with calcite crystals, monitored in situ[5−9] as well as the development of theoretical models.[10−12] The effect of inorganic impurities on both crystal growth and dissolution has been investigated using in situ atomic force microscopy (AFM) experiments[13−20] and by atomistic simulations.[21,22] In a recent review, Morse et al.[23] addressed the major aspects of carbonate mineral formation and dissolution in the marine environment and underlined the controlling factors of temperature, pressure, and salinity on the saturation state of seawater with respect to such minerals. Considerable attention has also been given to the investigation of biological interactions of organic acids and proteins with calcite substrates as a first step toward the understanding of biomineralization phenomena and also demineralization processes.[24−26]

Among naturally encountered ion "impurities" present in the growth and/or dissolution environment of calcitic materials is fluoride. Naturally occurring fluoride exists in trace amounts in almost all ground waters (<4 mg·L^{-1}), surface waters (0.1−0.3 mg·L^{-1}), and marine waters ($\sim$1 mg·L^{-1}).[27−29] Elevated fluoride levels have been reported to be present in industrial wastewaters (e.g., thermal power plants, fertilizer production). Since the 1960s fluoride compounds (up to 1 mg/L) have been added to municipal drinking water supplies in a number of urban areas as a preventive approach toward health (i.e., dental, skeletal).[30,31] Fluoride may also adsorb onto geomaterials[32] including carbonate minerals.[33−36] Earlier reports have shown that fluoride ions present in the aqueous phase may interact with calcite crystals.[37−39] Investigation of the interaction of the fluoride ions at the calcite−water interface at the nanoscale is the key to understand their role at the solid/fluid interface. Of particular interest is the investigation of the role of fluoride ions present in the aqueous environment of the supersaturated and undersaturated solutions from which calcium carbonate is crystallized or dissolved, respectively.

In the present work we report on an AFM study of the interaction between calcite $\{10\bar{1}4\}$ surfaces and F-containing aqueous solutions. The study aims at highlighting important

*Corresponding author. E-mail: kvavouraki@chemeng.upatras.gr. Tel./Fax: +49-251-833-3454/ +49-251-833-8397.

changes in mineral surface features, contributing to a better understanding of the mechanisms of F^- ions' interaction with calcite surfaces. In situ AFM experiments were carried out for the investigation of the effect of the presence of fluoride ions in supersaturated and undersaturated solutions during both growth and dissolution of calcite crystal surfaces.

II. Materials and Methods

Experimental Solution Speciation. All experiments were carried out at room temperature (23 ± 1 °C). Calcium chloride, sodium carbonate, and sodium fluoride stock solutions were prepared from the respective crystalline solids (Merck, puriss p.a., ACS reagent, ≥99%) without any further purification. Calcium solutions were analyzed by inductively coupled plasma optical emission spectrometry (ICP-OES, Atom Scan 25 Thermo Jarrell Ash). The supersaturated and undersaturated solutions were prepared by mixing equal volumes of calcium and carbonate solutions from the respective stock solutions. The pH of solutions was measured using a combination glass − Ag/AgCl (3 M KCl) electrode (PH-BTA by Vernier) calibrated with 7.00 and 10.00 buffer solutions (Schott Gërate). The solution speciation and saturation state (S.I.) calculations in the supersaturated and undersaturated solutions were made using the PHREEQC software.[40] The saturation with respect to the calcite phase is expressed as the saturation index (S.I.) by eq 1:

$$\text{S.I.} = \log \Omega = \log(\text{IAP}/K_{sp}) \quad (1)$$

where Ω is IAP/K_{sp}, IAP is the ion activity product, and K_{sp} the corresponding thermodynamic solubility product of calcite ($\log K_{sp} = -8.48$).[41]

The species involved in the system included H^+, HO^-, H_2O^0, H_2, O_2, HCO_3^-, CO_3^{2-}, $CaCO_3^0$, $CaHCO_3^+$, $NaCO_3^-$, $NaHCO_3^0$, Ca^{2+}, $CaOH^+$, Na^+, $NaCO_3^-$, $NaOH^0$, and Cl^-. In the presence of fluoride the additional species of F^-, NaF^0, HF^0, HF_2^- and CaF^+ were taken into consideration in the calculations. The solubility product of fluorite is $\log K_{sp} = -10.60$.[42] PHREEQC was also used to calculate the appropriate concentration of calcium chloride, sodium carbonate, and sodium fluoride in the solutions to maintain constant supersaturation with respect to calcite when fluoride is present. In the growth experiments in the presence of 5 mM of fluoride, the calcium and carbonate concentrations were higher (0.38 mM) in order to keep the same supersaturation (see Results), taking into account possible ion pairing. The supersaturation index S.I. with respect to calcite was calculated to be 0.89. This value ensured measurable in situ growth rates.[19,20] The experimental conditions for the crystal growth experiments are summarized in Table 1. The S.I. values with respect to the fluorite phase for each dissolution experiment and the number of discrete samples tested are summarized in Table 2.

Two series of calcite dissolution experiments in undersaturated solutions with respect to calcite were carried out. For dissolution experiments CO_2-free solutions of $CaCl_2$ and NaF were prepared (supersaturated with respect to fluorite). The molar total calcium (Ca_t) to total fluoride (F_t) was 2 and fluoride concentrations varied in the range between 0.4−2 mM. The maximum value of the S.I. with respect to fluorite was calculated to be 2 corresponding to NaF concentration of 2 mM (exp. no. 17). Experiments at higher fluoride concentrations used solutions with no added calcium (to prevent fluorite precipitation in the working solution (exp. nos. 18−21, Table 2)).

Table 1. Experimental Solution Conditions of Calcite Crystal Growth in the Absence and in the Presence of Fluoride[a]

experiment no.	pH	S.I.$_{calcite}$	S.I.$_{fluorite}$	NaF (mM)	no. of samples
1	10.2	0.89	0[a]	0	2
2	10.2	0.89	−2.27	0.025	1
3	10.2	0.89	−1.67	0.05	2
4	10.2	0.89	−1.07	0.1	1
5	10.2	0.88	−0.47	0.2	2
6	10.2	0.88	−0.04	0.33	2
7	10.2	0.86	0.72	0.8	2
8	10.2	0.83	1.49	2	2
9[c]	10.2	0.89	2.28	5	2

[a] Total calcium (Ca_t) = total carbonate (C_t) = 0.33 mM, (23 °C). Initial pH values, saturation index (S.I.) for calcite and fluorite, concentration of sodium fluoride in the supersaturated solutions and the number of different calcite samples used for the measurements of the crystal growth rates. [b] Solutions with values of S.I. = 0 are saturated; S.I. > 0 supersaturated; S.I. < 0 undersaturated. [c] Total calcium (Ca_t) = total carbonate (C_t) = 0.38 mM.

Table 2. Experimental Solution Conditions of Calcite Dissolution in the Presence of Fluoride[a]

experiment no.	pH	S.I.$_{fluorite}$	$CaCl_2$ (mM)	NaF (mM)	no. of samples
10	7.1	0.01	0.2	0.4	1
11	7.1	0.52	0.3	0.6	2
12	7.2	0.87	0.4	0.8	1
13	7.2	1.02	0.45	0.9	2
14	7.2	1.15	0.5	1	1
15	7.2	1.27	0.55	1.1	2
16	7.2	1.73	0.8	1.6	1
17[b]	7.3	2	1	2	1
18	7.2	−	−	1.1	2
19	7.3	−	−	2	1
20	7.8	-	-	40	1
21	7.9	−	−	50	2

[a] Measured pH values, saturation index with respect to fluorite, concentrations of calcium chloride and sodium fluoride in the solutions and respective number of calcite samples used for the dissolution rate measurements. [b] Additional solution preparation of 5 mM $CaCl_2$ and 10 mM NaF resulted in spontaneous precipitation of CaF_2.

In Situ AFM. All experiments were carried out using a Digital Instruments Nanoscope III Multimode AFM equipped with a fluid cell at room conditions (23 °C and 1 atm). Prior to the experimental runs, the AFM scanner was calibrated in the x, y, and z directions, to ensure accurate voltage to nm conversion. The observations were made in contact mode over freshly cleaved calcite surfaces, and the scanned areas were either 6 × 6 μm or 10 × 10 μm (for most experiments). Optically clear Iceland spar calcite crystals (from Mexico) were cleaved directly before each experiment and used as substrate material (3 × 2 × 1 mm) for the crystal growth and dissolution experiments. The scan time for each image was approximately 1.5 min and the scan rate was 3.05 Hz. AFM images were taken at the end of each scan after which fresh solution was injected into the AFM fluid cell to give an effective flow rate of 0.66 mL min^{-1}. The selected flow rate through the cell was sufficient to ensure that the growth and dissolution mechanisms were surface controlled.[43] The experimental conditions at the flow cell system were such that they ensured a closed system, without exchange of CO_2 with the atmosphere. The continuous renewal of the working solution in the cell and the very small solid

surface area to solution ratio resulted in the maintenance of the S.I. with respect to calcite throughout the experiments. The total duration of each growth and dissolution experiment was approximately 1 h. During this time period, a number of etch pits (4−5) on the calcite crystal surface were monitored. The AFM sequential images provided information on the rates of the growth and dissolution processes, as well as the crystallographic orientation and the height of the advancing or receding steps on the calcite surface in the presence of supersaturated and undersaturated solutions, respectively. Microtopographic features of the changing surface of the calcite crystal were obtained at various stages of the growth and/or dissolution processes.

Before crystal growth and dissolution experiments, the cleaved calcite surfaces were exposed to deionized water (resistivity 18.2 MΩ cm^{-1}, Milli-Q) flowing through the AFM fluid cell and the dissolution of the $(10\bar{1}4)$ calcite surface was recorded. The dissolution rate in these experiments is defined as the velocity of calcite step retreat and was measured for each surface prior to injecting the experimental solution. The passage of water over the surface removed particles generated by the cleaving the crystal and produced rhombohedral etch pits. The etch pits are bounded by 2 pairs of nonequivalent steps with orientations parallel to $[\bar{4}41]_+$, $[48\bar{1}]_+$, $[\bar{4}41]_-$, and $[48\bar{1}]_-$ directions. The steps with subscript + are differentiated from those with subscript − as they form obtuse and acute angles, respectively, with the cleavage plane. Furthermore, the pair of obtuse steps has a faster spreading rate than the acute steps. Etch-pit spreading and closure rates were measured along the two bisector directions [010] and $[42\bar{1}]$. To take into account the anisotropy of the step velocities and changes in the shape of etch pits, step propagation (or retreat) velocity measurements were made by measuring the rate of change in the length of the bisectors of the etch pits in the [010] and $[42\bar{1}]$ directions (Figure 1a). The depth of the pits was either ~3 Å or ~6 Å, corresponding to the depth of one or two $CaCO_3$ unit cell layers parallel to this plane. Introduction of each new batch of supersaturated or undersaturated solution resulted in the growth or retreat of steps on the surface of the calcite crystals. Step velocity was calculated in each case from a sequence of images over a time period in order to optimize statistically the measured values. The crystal growth rates, both in the absence and in the presence of fluoride ions, were measured from the time dependence of the closure of the rhombohedral etch pits and from the rates of the development of new nuclei in the same [010] direction. The molar total calcium (Ca_t) to total carbonate (C_t) ratio in the supersaturated solutions was equal to 1. Kinetics measurements[44,45] based on the Kossel kinetic model of crystal growth[46] suggested that at constant supersaturation, the growth rate of step propagation of various crystal faces reached a maximum value corresponding to a cation to anion molar concentration ratio equal to one. A total of eight crystal growth experiments were done in duplicate at the same supersaturation. The duplicate experiments were done using two different, freshly cleaved calcite surfaces. For the dissolution rate measurements, the [010] and $[42\bar{1}]$ diagonal lengths on the dominant $(10\bar{1}4)$ calcite cleavage faces were determined using the Nanoscope III software. The etch pit formation on the calcite crystal surface and the respective habit modification was mapped, and dissolution rates were measured in a series of experiments in which the undersaturated solutions consisted of calcium chloride containing various concentrations of sodium fluoride. It should be noted that in the literature the diagonal $[42\bar{1}]$ is often incorrectly cited as $[2\bar{2}1]$.[47]

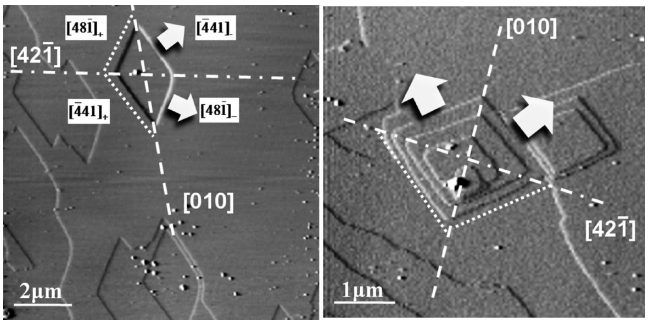

Figure 1. AFM deflection image of a calcite surface exposed to (a) deionized water and (b) a supersaturated solution with respect to calcite. Solid arrows show the obtuse (fast) steps along the crystallographic directions of $[\bar{4}41]_+$, $[48\bar{1}]_+$ and $[\bar{4}41]_-$, $[48\bar{1}]_-$ (dotted lines) of rhombohedral nuclei development as well as the [010] and $[42\bar{1}]$ directions (dashed lines).

III. Results

Nanoscale Measurements of Calcite Growth. Successive AFM images of both growth and dissolution experiments were obtained after partial calcite water dissolution. For all AFM experiments, the spreading rate in deionized water from the change in length of the etch pit along the [010] and $[42\bar{1}]$ directions had an average value of 2.6 nm/s (±0.7) and 1.7 nm/s (±0.7), respectively. In fluoride-free solutions during growth, etch pits were closed at considerably slower rates in comparison with the growth of two-dimensional nuclei. Different velocities of etch pit closure and nuclei growth in the [010] direction were measured to be 4.1 nm/s (±0.8) and 6.1 nm/s (±1.2), respectively. The values of the rates measured were of the same order of magnitude with values reported for calcite growth at the same experimental conditions.[19,20] In calcite growth measurements, most of the rhombohedral etch pits and step edges were completed with growth along the $[44\bar{1}]$ and $[48\bar{1}]$ crystallographic directions. A few particles, possibly debris, present as a result of the sample preparation procedure, attached onto the calcite surface, initiated the secondary nucleation of two-dimensional (2-D) islands.[48] The 2-D nuclei followed a similar growth pattern as the closure of etch pits on the same surface. Figure 1 depicts the calcite surface features developed during growth. Both etch pit closing (Figure 1a) and individual nuclei growth (Figure 1b) were observed. The arrays of calcite steps show the calcite growth along $[\bar{4}41]_+$ and $[48\bar{1}]_+$ directions (Figure 1a). The height of each individual step was approximately 3 Å, corresponding to the height of a $CaCO_3$ monolayer. The slight rounding and local irregularity of monolayer steps between obtuse steps are similar to features reported from previous real-time AFM studies of calcite growth on cleavage surfaces.[7,48−50]

Effect of Fluoride on the Crystal Growth of Calcite. The presence of fluoride in the solutions supersaturated with respect to calcite, resulted in the modification of the morphology both of the etch pits and of the new nuclei. During growth at low fluoride concentrations (0.025−0.33 mM) the etch pits, formed during the specimen water pretreatment, closed in the same crystallographic orientations as in the growth of calcite in the absence of fluoride. However, the 2-D calcite nuclei advancing in the same direction, showed

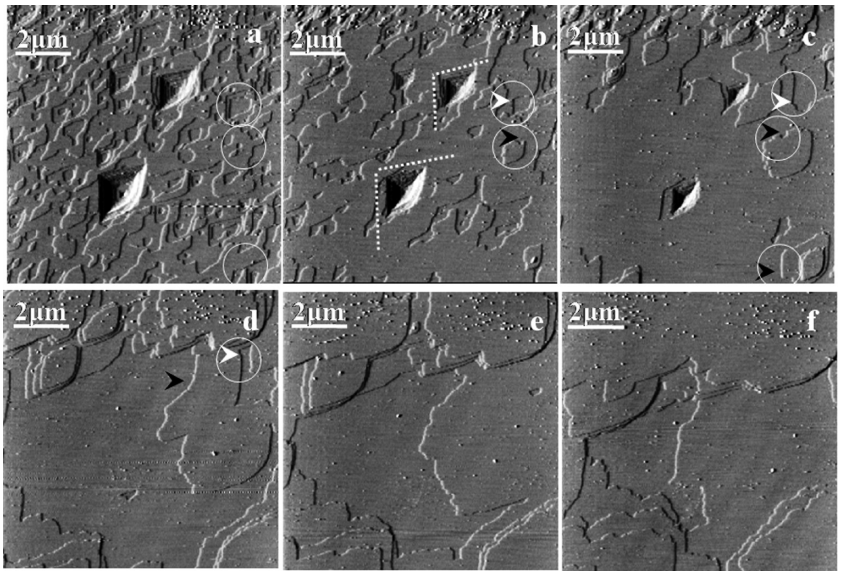

Figure 2. AFM deflection images of a calcite growth sequence in 0.33 mM $CaCl_2$ and Na_2CO_3 solution pH 10.2, 23 °C in the presence of 0.1 mM NaF. (a) $t = 0$, (b) $t = 3$ min, (c) $t = 6.5$ min, (d) $t = 11.5$ min, (e) $t = 14.5$ min, (f) $t = 20$ min, scan size $10 \times 10\,\mu$m. Arrowheads refer to phenomena of interest described in the text.

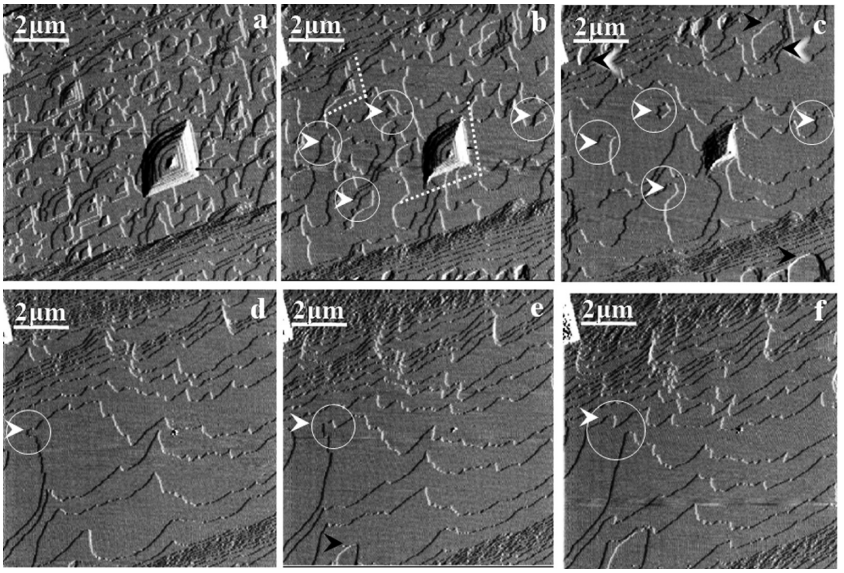

Figure 3. AFM deflection images of a calcite growth sequence in 0.33 mM $CaCl_2$ and Na_2CO_3 solution, pH 10.2, 23 °C in the presence of 2 mM NaF. The new growth step edges are irregular and pinned in comparison with the calcite growth in the absence of fluoride. (a) $t = 0$, (b) $t = 6$ min, (c) $t = 11$ min, (d) $t = 26$ min, (e) $t = 37$ min, (f) $t = 52$ min, scan size $10 \times 10\,\mu$m. Arrowheads refer to phenomena of interest described in the text.

differences both in the mechanism and in the rate of growth. Figure 2 shows representative AFM deflection images of a calcite growth sequence from supersaturated solutions containing 0.1 mM NaF. Both shallow and deep etch pits were present on the growing crystal surface (Figure 2a−c) and the pattern of pit closure was the same as the initial rhombohedral step directions (dotted lines, Figure 2b). The reproduction of the previous etch pit shape (circled area indicated with white arrowheads) was also observed. In the presence of fluoride ions, the newly grown monolayers developed in a manner such that the calcite surface was covered exhibiting the former etch pit pattern. This is referred to as the "Template effect".[51] In addition to etch pit morphological observations, nuclei development steps were less regular and more curved in the presence of fluoride (Figure 2c,d). The acute step edges of new nuclei remained straight, while the obtuse step edges had the same curvature as the closing etch pit (circled area indicated with black arrowheads, Figure 2c). The new emerging nuclei (Figure 2d) followed the acute step edges of a former deep etch pit. The crystal growth rates were calculated to be 3.3 nm/s (±0.7) for the etch pit closure and 4.4 nm/s (±1.0) for the growth of the 2-D nuclei on the calcite surface. The first value was comparable to fluoride-free solutions (within the experimental error). The second value showed a decreasing trend of the rate as a function of time.

In excess of 0.33 mM fluoride in the supersaturated solutions, the kinetics of calcite crystal growth changed. Figure 3 shows a sequence of images at high fluoride concentrations (≥0.8 mM NaF). For a supersaturated solution containing 0.33 mM $CaCl_2/Na_2CO_3$ and 2 mM NaF

(S.I. = 0.85), the etch pits filled along crystallographic directions (dotted lines point out $[\bar{4}41]_+$ and $[48\bar{1}]_+$ directions, Figure 3b) and the growth rate along [010] was reduced to 2.3 nm/s (±0.9). During the crystal growth process, the original topography of the etch pit reappeared (circled area indicated with white arrowheads, in Figure 3b−f). During the growth of the 2-D nuclei, the obtuse and acute steps merged and formed rounded corners (black arrowheads, Figure 3c,e). The acute steps remained slightly rounded in comparison with the respective situation in the absence of fluoride, where the obtuse steps became more irregular (black arrowheads in shadow, Figure 3c). The new nuclei formed on the growing calcite surface turned into rounded shapes and the respective average growth rate was 2.3 nm/s (±0.7) in the [010] direction. The step velocities of nuclei decreased significantly in the presence of 2 mM aqueous fluoride. Advancing steps resulted in the coverage of the original surface. However, pinned-shape steps suggested retardation of the growth process. Figure 4 shows a plot of the growth rates of both etch pit closing and nuclei spreading in the [010] direction in the presence of fluoride in the supersaturated solutions in comparison with the respective observations in the absence of fluoride (dashed and dotted lines). Moreover, the advancing steps during the growth of the 2-D nuclei, exhibited increased edge roughness, suggesting interaction of the calcite surface with a fluoride species at these positions, possibly by step pinning.

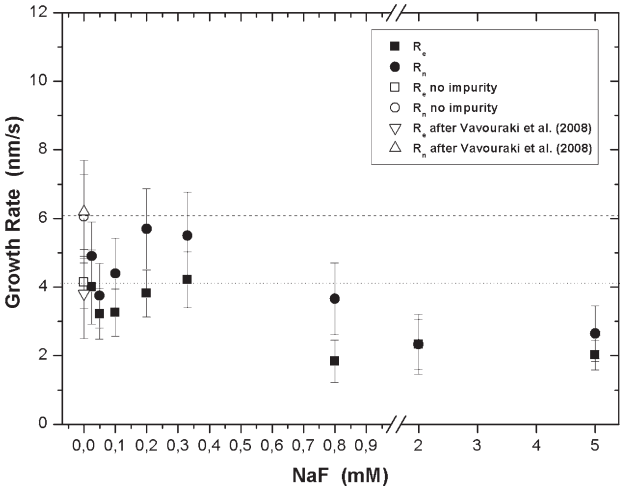

Figure 4. Rates of closure of etch pits (R_c) and nuclei spreading (R_n) during calcite growth in the presence of fluoride. Dashed line (---) for nuclei development rate and dotted line (···) for the rate of closing of the etch pits depicts the growth rates in the absence of fluoride ions. Experimental conditions are shown in Table 1.

Calcite Dissolution. Although the number of calcite specimens tested was limited, the data showed systematic changes in step retreat during dissolution. In the presence of low fluoride concentrations (0.4−1.1 mM), dissolution resulted in changes of the etch pit morphology. The rhombohedral calcite etch pit morphology changed to hexagonal-like. The increase in the [010] diagonal direction (Figure 5b) was slower in comparison with the respective rate in the $[42\bar{1}]$ direction. AFM deflection images, shown in Figure 5, illustrated the etch pit transformation following exposure of the calcite surface to the fluoride solution. Both sharp obtuse-acute step corners of calcite etch pits were converted to straight step edges in the $[42\bar{1}]$ direction (dashed line Figure 5d). The dissolution rates measured were 4.2 ± 0.8 nm/s and 3.4 ± 0.7 nm/s in the $[42\bar{1}]$ and [010] directions, respectively. Dissolution rates in the presence of 0.4 mM NaF increased 60% along $[42\bar{1}]$ and 40% along the [010] direction with respect to the corresponding values in pure water.

A similar trend for the rates of dissolution was found for higher concentrations of fluoride (0.6 to 1.1 mM) in the undersaturated solutions. At concentration levels exceeding 1.6 mM NaF, the rate of calcite dissolution decreased. Figure 6 shows the formation of sharp, intersecting steps on the dissolving calcite surface in the presence of 1.1 and 2 mM NaF (dotted lines Figure 6Ia, IId). The etch pit morphology changed from rhombohedral to hexagonal along the $[42\bar{1}]$ direction (dashed lines; Figure 6Ib, IIe) after a few minutes of exposure to the solution. The dissolution rates were 5.3 ± 0.6 nm/s and 2.8 ± 0.4 nm/s in the $[42\bar{1}]$ (70% increase) and [010] directions, respectively. In the presence of 2 mM NaF (Figure 6II) etch pit edges were modified exhibiting small curvatures in the $[42\bar{1}]$ direction (Figure 6IId to f). During the course of the step retreat during dissolution of the calcite crystal surface, the density of etch pits on a calcite surface increased significantly (Figure 6IId). The dissolution rate was 0.7 ± 0.3 nm/s in the [010] direction. The rate in the $[42\bar{1}]$ direction was approximately equal to the rate measured in deionized water (1.7 ± 0.9 nm/s). Figure 7 shows a plot of the rates of dissolution from etch pit spreading as a function of NaF concentration. Although most of the solutions used in the dissolution experiments were supersaturated with respect to CaF_2 (Table 2), no fluorite growth was seen on the calcite surface.

In a second series of experiments, the dissolution of calcite crystals was investigated using solutions of sodium fluoride (i.e., CO_2-free solutions without added Ca). In all cases, pH was ~7.2, whereas at higher fluoride concentrations (40 and 50 mM NaF) the solution pH was 7.8. With an exception of one AFM experiment with $CaCl_2$ solution of 0.55 mM

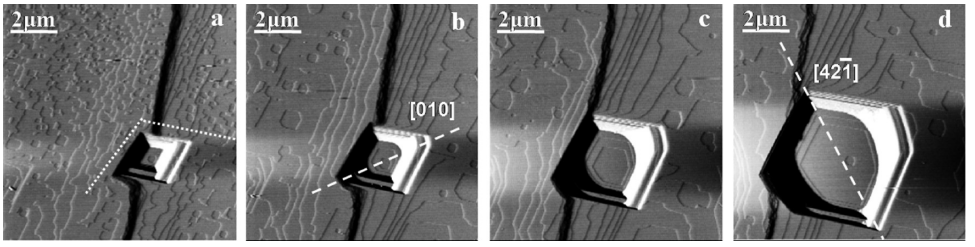

Figure 5. AFM deflection images of a calcite dissolution sequence in solutions containing 0.8 mM $CaCl_2$ and 0.4 mM NaF, pH 7.2, 23 °C. Acute−acute steps are designated with dotted lines. Obtuse−acute corners developed into straight lines parallel to the $[42\bar{1}]$ direction (dashed line). (a) $t = 0$, showing rhombohedral etch pits developed in pure water (b) $t = 3$ min; depiction of [010] direction (c) $t = 8$ min (d) $t = 16$ min, scan size 10 × 10 μm.

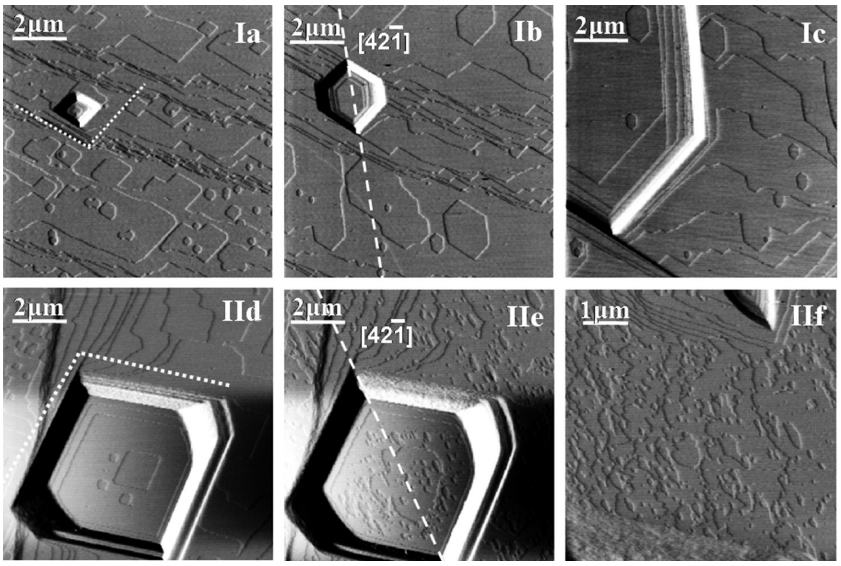

Figure 6. AFM deflection images of a calcite dissolution sequence in solutions (I) 0.55 mM $CaCl_2$ and 1.1 mM NaF, pH 7.2, 23 °C. (a) $t = 0$ (b) $t = 5$ min (c) $t = 40$ min, scan size 10×10 μm. (II) 1 mM $CaCl_2$ and 2 mM NaF at pH 7.3 and 23 °C. (d) $t = 0$ min (e) $t = 5$ min, scan size 10×10 μm, (f) $t = 47$ min, scan size 6×6 μm.

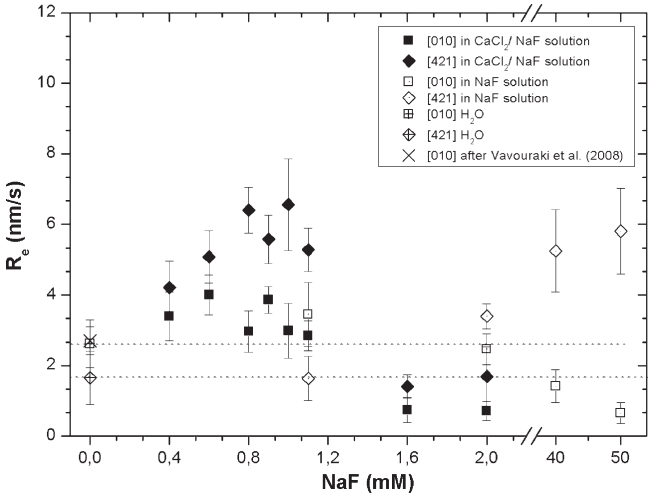

Figure 7. Rates of etch pits spreading in the [42$\bar{1}$] (■) and [010] (♦) directions during calcite dissolution in the presence of fluoride in $CaCl_2$ solutions (solid symbols) and in water (open symbols). A correlation of dissolution rates of etch pits in deionized water in the [42$\bar{1}$] and [010] directions (dashed and dotted lines, respectively) are also shown. Experimental conditions are shown in Table 2.

(pH = 7), rhombohedral etch pits were exhibited on the calcite crystal surface upon exposure to either calcium (0.55 mM $CaCl_2$) or fluoride (1.1 mM NaF) solutions. The sharp intersecting steps dissolved regularly in the [$\bar{4}$41] and [48$\bar{1}$] directions (dotted lines in Figure 8a,b). The appearance of rounded obtuse corners suggested differences in step velocities.[8,54] In the presence of 1.1 mM NaF, the etch pits spread out all over the surface while the step edges became rough (Figure 8b). At higher fluoride concentration (≥2 mM NaF) the etch pit habit was modified to hexagonal and the step recessions were markedly different in comparison with the respective cases in the presence of lower fluoride concentrations (Figure 8a,b). Both the etch pit density and depth increased when the fluoride concentration was significantly increased to 40−50 mM.

The nucleation of hexagonal etch pits on the calcite crystal surface in contact with the undersaturated (with respect to calcite) solutions containing fluoride was developed in the [42$\bar{1}$] direction (shown by the dashed line Figure 8c−e). The presence of fluoride ions (maximum value of 50 mM NaF) resulted in the increase of etch pit dissolution rate along the [42$\bar{1}$] direction by ∼70%. At the same time however, the dissolution rate was reduced by ∼60% in the [010] direction (Figure 7). The dissolution rates measured were compared to the dissolution of the test calcite crystals upon exposure to pure water. In the presence of sodium fluoride concentrations exceeding 2 mM, the rhombohedral etch pits changed to hexagonal shapes.

IV. Discussion

Calcite growth and dissolution processes observed in situ on the surface of a cleaved calcite crystal were directly recorded as monolayer step propagation or retreat and were probably initiated from dislocations or point defects within the calcite structure.[5,6,52,53] The nonequivalent crystallographic orientations of [$\bar{4}$41] and [48$\bar{1}$] steps depicts a rhombohedral shape of the unit cell which controls the rhombic shape of etch pit development over the surface. Two of the neighboring, intersecting steps forming a corner are "slow", termed as acute steps, while the diagonally opposite pair is "fast", or obtuse steps. The distinct differences in step velocities of opposed steps of acute and obtuse edges are consistent with previous experimental observations[5,6,8,52,54−56] and theoretical calculations.[11,12,22] Surface groups exposed at obtuse steps have more open configurations and offer greater accessibility to the solvent leading to faster motion of obtuse steps during pure dissolution and growth.[5,43,57] The ratio difference in velocities of anisotropic step retreat ranges from 2 to 4.[8,52,58,59] The value of etch pit step retreat along the [010] direction and the ratio of the lengths of etch-pit bisectors [42$\bar{1}$]/[010] (0.65 in this study) was comparable to previous studies.[19,20,47] The crystal growth rates measured in the supersaturated solutions were comparable with earlier reports for the kinetics of crystal growth of calcite at the same conditions.[19,20]

In situ AFM observations suggested that during calcite crystal growth and dissolution, the interactions between the

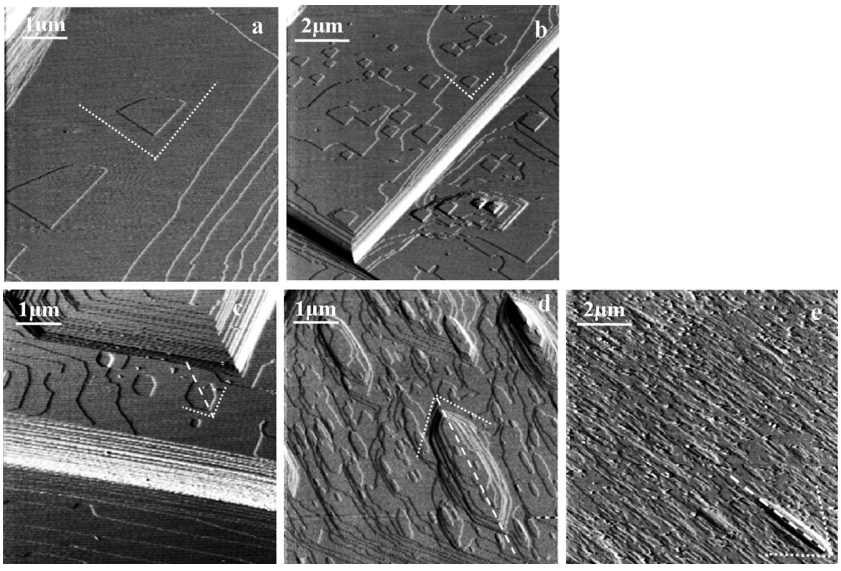

Figure 8. AFM deflection images of a dissolved calcite surface showing the obtuse steps orientation (dotted lines) in calcium solutions of (a) 0.55 mM $CaCl_2$ (scan size $6 \times 6\,\mu$m) and fluoride solutions of (b) 1.1 mM, scan size $10 \times 10\,\mu$m (c) 2 mM (d) 40 mM, both scan size $6 \times 6\,\mu$m and (e) 50 mM NaF, scan size $10 \times 10\,\mu$m, ca. 7 min after exposure to the undersaturated solutions at pH 7.3, 23 °C.

fluoride ions and the calcite surfaces takes place at the intersection of the $\{10\bar{1}4\}$ cleavage planes of calcite. It is possible that changes in the calcite surface morphology may be due to induced strain resulting from F incorporation at the intersections of nonequivalent step-types as suggested Davis et al.[60] They also observed a formation of pseudofacets with an orientation approximately parallel to the (010) face during calcite growth in the presence of Mg^{2+} suggesting that step-specific impurity interactions occur as a result of incorporated strain across step boundaries.

The presence of fluoride ions within the range of concentrations investigated in the present work altered both the step velocities and the step migration in comparison with the features exhibited in calcite growth in the absence of additives. For growth experiments at low fluoride concentrations (0.025−0.33 mM), the closure rates of etch pits was comparable to the respective values for calcite growth in the absence of additives at the same calcite supersaturation. The rates of growth however of 2-D nuclei showed a tendency toward lower values in the presence of fluoride. AFM sequential images showed the propagation of new growth layers and revealed etch pit locations present before the start of the crystal growth process. The etch pits initially present on the crystal surface, following the initial dissolution in pure water, fill with a new layer of different unit cell height. The etch pit edges function thus as obstacles to the growth of continuous new layers. Subsequent layers grow over the surface in the same manner. The original etch pit microtopography becomes thus a template for the overgrowing layers. This modality of step propagation and development termed the "template effect" may explain adequately the differences in the tendency of foreign ions to incorporate into a calcite crystal during growth.[19] This behavior strongly depends both on the composition of the aqueous solution and on the corresponding supersaturation of the solution with respect to the solid forming on the surface.[61,62] According to the impurity incorporation model, ions may be incorporated into the growing crystal during step propagation.[63] Surface steps are modified revealing potential impurity incorporation into the calcite lattice. The impurity incorporation occurs upon capture of foreign ions or molecules by advancing steps or otherwise they incorporate at kink sites along a step-edge to become part of the growing or dissolving crystal. If the step propagation energy is lower than the bond energy between adjacent growth units, the crystal solubility may increase resulting in the reduction of the effective supersaturation and reduced step velocity.

The presence of impurities in the supersaturated solutions affects crystal growth rates, crystal morphology, and the thickness of the growth layers.[51,64] Measured nuclei growth rates were ~20% higher than the rates of the closure of etch pits at the same supersaturation. The supersaturation with respect to calcite in the experiments in the present work was sufficiently high (S.I. = 0.89) for nuclei development to dominate the overall growth rate.[48] Spreading nuclei may exhibit the template effect as well in the first few layers, while growth steps on the calcite surface were irregular and curved. Possible incorporation of fluoride into the calcite lattice depends on the concentration of the fluoride ions in solution. However, the growth layer thickness remained at 3 Å as in the case of calcite crystal growth in the absence of additives. The presence of divalent ions such as barium, manganese, and strontium has been reported to reproduce the original surface microtopography of calcite monolayers developed during crystal growth.[19,20,51,65,66] However, in situ AFM studies on calcite in the presence of strontium, magnesium, and aspartate did not report changes in the step height during crystal growth[67,68] and dissolution of calcite.[69]

Higher fluoride concentrations (≥0.8 mM NaF) during calcite growth reduces both the rate of pit closure and the rate of nuclei spreading in the [010] direction (ca. by 50%) resulting in staggered step propagation. The step growth velocity (either obtuse or acute) is related to the effective supersaturation.[1,70] Decrease of the effective supersaturation may result in the significant retardation of step advancement due to fluoride incorporation. The solubility of the new phase of calcite containing fluoride is higher than the value corresponding to calcite ($K_{sp} = 10^{-8.48}$) and higher in comparison with fluorite ($K_{sp} = 10^{-10.60}$). It has been argued that the increased apparent solubility of a solid-solution of fluoride in calcite leads to a decrease of the effective supersaturation

with respect to calcite and consequently growth rates are retarded.[60,67] However, this argument is not thermodynamically valid, as it does not follow that an increase in solubility due to solid solution formation results in a decrease of the effective supersaturation. An aqueous solution can be undersaturated with respect to a pure end member but supersaturated with respect to a more soluble solid solution composition.[71,72]

The evolution of new growth steps over a calcite surface leads to a more irregular and rough topography compared to pure calcite growth. Both the new growth layers reproducing original surface microtopography and the advancement of 2-D nuclei results in the formation of jagged and pinned edges, as observed earlier. The classic model of step pinning[73] may explain the morphology difference from straight-line growth along crystallographic directions to pinned step growth. Previous observations studied ion−calcite surface interactions and showed attachment onto growth steps.[7,74−76] AFM deflection images of calcite growth in the presence of strontium and sulfate ions showed roughening and pinning of calcite step edges and/or kink sites which were interpreted as the result of step "poisoning" from these ions.[19,20,68] A step-specific kinetic mechanism may explain the retardation of the growth of calcite in the presence of fluoride as due either to the pinning of the steps by F^- ions through adsorption at the step edges followed by their incorporation into the overgrowing steps, or because of the binding of F^- ions to terraces. Both step velocity measurements and the type of step advancement demonstrate that aqueous fluoride probably incorporated into the calcite crystal structure during the growth process. Because of irregular step edges, the pinning effect model may be applicable.[73] Although solutions with relatively high fluoride concentrations were supersaturated with respect to both calcite and fluorite, the latter phase was not observed on the calcite surface.

Previous macroscopic experiments on calcite interactions with fluoride solutions have shown that epitaxial growth of fluorite on calcite is favorable, with the Ca-net on the (110) plane of fluorite coinciding with that on the cleavage plane of calcite.[77] The absence of epitaxial nucleation of fluorite on the calcite surface, from solutions supersaturated with respect to fluorite may be due to the relatively long induction time for nucleation which is disproportional to the time scale used in the present series of experiments. A potential epitaxial growth of fluorite on the calcite surface may occur at higher supersaturation values ($S.I._{fl.} \gg 2$) with respect to fluorite, but this is beyond the scope of this paper.

Dissolution rate measurements were compared with the respective rates of dissolution in [010] and [42$\bar{1}$] directions (Figure 7). As may be seen in Figure 7, there was a significant difference in the measured rates at low and high fluoride concentration. In addition to rate differences, significant etch pit morphological differentiation was found in the two concentration ranges (low-high) investigated. In situ measurements of parameters such as solution composition, degassing (CO_2), or the presence of impurities are impossible to quantify but likely to contribute to overall errors.[68] Absolute rates may be changed, but the relative behavior remained constant allowing comparison of relative differences in step retreat rate between samples.[78]

A significant result that emerged from the current AFM dissolution study was the alteration of the etch pit morphology during the interaction of fluoride ions with the calcite surface. The evolution of etch pits was modified along the [42$\bar{1}$] direction. Such a modification suggests that fluoride interacts differently with the nonequivalent steps of calcite and the F^--ions are adsorbed at the step edges or at the kink-sites. At low fluoride concentrations ($\leq$1.1 mM NaF), the rates of etch pit spreading in the [010] direction remained constant (within experimental error). The rates of dissolution however in the [42$\bar{1}$] direction increased by ca. 70% promoting the formation of hexagonal shaped etch pits. Comparable studies have revealed similar surface-modifying etch pit features. The formation of modified rhombohedral to triangular shaped etch pits and hillocks has been reported during calcite dissolution in the presence of aspartate.[69] The formation of semitriangular etch pits has been observed in the presence of aqueous cobalt and was attributed to the adsorption of cobalt at the negative (acute) kinks and/or edges.[16] The adsorption of heavy metal impurities on calcite has been reported to favor the formation of arrays of deep triangular etch pits which outgrow to form interconnected larger hexagonal or elongated oval etch pits.[14,15,35] Similar, yet faster etch pit modification to hexagonal and/or a pseudoelliptical shape in the [42$\bar{1}$] direction has been reported for the dissolution of calcite in solutions containing cadmium and maleic acid.[47,79] The morphological changes observed in the present work, during the dissolution of calcite in the presence of fluoride, resulting in the hexagonal elongation of the etch pits, may be possibly attributed to the interaction of ion pairs formed between the fluoride and calcium ions. Calcium ions exposed along the step sites in the cleavage plane may be bridged with fluoride ions. Pérez-Garrido et al.[47] suggested a preferential incorporation of Cd-impurity at specific acute steps, while obtuse steps become coarsely scalloped. In the present investigation, both (obtuse/ acute, ±) corners of acute [$\bar{4}$41] and [48$\bar{1}$] steps were preserved. Sharp corners imply that interactions with F^- take place at both acute and obtuse steps edges. In all studies,[15,49,79] step features show faster recession in the [42$\bar{1}$] rather than the [010] direction, in agreement with our results.

At higher fluoride concentrations (1.6 and 2 mM NaF), the dissolution rates in [42$\bar{1}$] and [010] directions were reduced. It should be noted that in this case the supersaturation value with respect to fluorite was higher ($S.I._{fl.}$ = 1.73 to 2), in comparison with the rest of the calcite dissolution experiments. Possible spontaneous precipitation of fluorite in solution[80] causing reduction of the dissolution rates because of the lower free fluoride concentrations present in the resulting undersaturated solution may have occurred. The etch pits spread over the calcite surface and exhibited a hexagonal form, slightly curved at the edges. Additional dissolution experiments were carried out in which the calcite crystals were allowed to dissolve in solutions containing only sodium fluoride solutions (1.1, 40, and 50 mM). For high fluoride concentrations (40 and 50 mM NaF), the dissolution rates in the [42$\bar{1}$] direction were faster and the calcite surface morphology exhibited a network of interconnected elongated hexahedral etch pits (Figure 8d,e). Thus, the total amount of step edges and/or roughness was significantly larger than the corresponding formations when dissolution of the calcite surface was measured in pure water.

Experimental studies[8,18,47] and molecular dynamics simulations[22] concerning measurements of growth and/or dissolution rates have shown that in the presence of ionic impurities in solutions in contact with the calcite surface, the steps undergo modifications. Becker et al.[81] addressed the issue of the effect of background electrolyte ions on the environment of the surface and on the precipitating ions. Both experimental and theoretical methods were used to determine the

interactions of single monovalent ions on the growth and dissolution rates of minerals consisting of divalent ions. Monovalent ions of the background electrolyte may change the morphology of growth features such as growth islands and spirals. Both Na^+ and Cl^- promote growth and dissolution of some crystals containing divalent metal ions, such as calcite, Barite and celestite. In solution all ions will be surrounded by a solvation layer of water molecules. Molecular dynamic simulations by Piana et al.[82] show that an ordered and tightly bound layer of water molecules present on a crystal surface means that if an ionic species approaches that surface, both the surface and ionic species have to be desolvated before the formation of new bonds; that is, growth, can occur. In general, the addition of foreign ions to a solution perturbs the solvation environment of the other ions present as well as the solvation of the crystal surface, and so in principle can affect the rates of surface processes such as dissolution and growth. F adsorption onto calcite surfaces, and consequent competition for hydration water, may cause a reduction in the energy barrier for 2-D nucleation of an etch pit, due to the surface destabilization associated with the disruption of the calcite surface hydration layer. This could explain the observed increase in etch pit density in the presence of F ions.

Recent AFM experiments by Kowacz et al.[83,84] have also shown that growth rate and nucleation are strongly affected by the solvation environment, which can be significantly modified by additives. The effect of electrolytes on the growth and dissolution kinetics of barite is based on the ability of ions to modify solvent structure dynamics and solute hydration. Different background ions have different hydration energy. This suggests that changes in the morphology of dissolution features can also be related to changes in the hydration of building units due to the presence of foreign ions in solution, in contrast with the commonly accepted view of specific interactions with active sites on mineral surfaces. It seems likely that mineral dissolution and growth from aqueous solutions is governed by a complex interaction between changes in solvent structure, surface hydration, and the ion solvation environment induced by the presence of electrolytes, as well as the surface characteristics of the dissolving or growing mineral.

Further experimental investigations by Kowacz et al.[84] revealed that hydrated impurity Na^+ ions were incorporated from the fluid phase into the crystal structure depending on the solution composition. However, Turner et al.[35] suggested that roughness and irregularity of etch pit morphology through calcite dissolution was the result of the presence of F^-, instead of Na^+. Na^+ incorporation during calcite growth may be simple occlusion or trapping in crystal defects or perhaps in fluid inclusions.[85,86] Na^+ however may also occupy interstitial positions in the calcite crystal.[87] The number of crystal defects in a calcite crystal determines the amount of incorporation of sodium into the calcite structure.[88] However, previous AFM growth[19,20] and dissolution experiments in the absence of fluoride and presence of sodium show no change in the etch pit morphology. Therefore it seems logical to attribute the observed changes described here to the presence of aqueous fluoride.

V. Conclusions

The presence of F ions in solution in contact with calcite surfaces during both growth and dissolution processes results in changes in the kinetics of the process as well as changes in both the morphology and the nucleation density of dissolution features. The crystal growth and dissolution rates in the presence of fluoride ions were significantly different in comparison to the corresponding experiments in their absence. During calcite growth experiments in the presence of low aqueous fluoride (0.025−0.33 mM) at constant supersaturation with respect to calcite and high pH, step advancement was comparable to pure calcite growth. However, at higher fluoride concentration (≥0.8 mM NaF), the rates of etch pit closure and nuclei spreading in the [010] direction are reduced by 50%) resulting in irregular steps and the pinning of step propagation. Some surface sites appeared blocked by the presence of fluoride impurity ions. During dissolution experiments in the presence of low aqueous fluoride (≤1.1 mM NaF) rates of dissolution in the [42$\bar{1}$] direction increased by ca. 70% promoting the formation of hexagonal shaped etch pits. At higher fluoride concentrations (1.6 and 2 mM NaF), a decrease (∼60%) in the dissolution rates in [42$\bar{1}$] and [010] directions was observed possibly because of a decrease in solubility. In the presence of a highly concentrated NaF solution (up to 50 mM), dissolution rate measurements in the [42$\bar{1}$] direction increased by 70%. The higher the fluoride concentration the rougher the terraces and more elongated step edges in the [42$\bar{1}$] direction were revealed. The resulting distortion of the local calcite structure leads to a modification indicating possible incorporation of fluoride into the bulk calcite structure. These results are significant for the understanding of calcite growth and dissolution in natural and industrial waters, where F ions may be present.

Acknowledgment. This project was supported by a Marie Curie Fellowship at the University of Münster (EU Early Stage Training Network MIR: Mineral−fluid Interface Reactivity, Contract No. MEST-CT-2005-021120). The authors appreciate technical help of Veronika Rapelius with ICP-OES analyses and acknowledge comments by three anonymous reviewers.

References

(1) Burton, W. K.; Cabrera, N.; Frank, F. C. *Phil. Trans. Roy. Soc. London A* **1951**, *243*, 299–358.
(2) Morse, J. W.; Arvidson, R. S. *Earth-Sci. Rev.* **2002**, *58*, 51–84.
(3) Reeder, R. J. *Geochim. Cosmochim. Acta* **1996**, *60*, 1543–1552.
(4) Koutsoukos, P. G.; Klepetsanis, P.; Spanos, N.; Kanellopoulou, D. G. *NACE Int. Corrosion Conf. Expo* **2007**, *07052*, 1–17.
(5) Hillner, P. E.; Gratz, A. J.; Manne, S.; Hansma, P. K. *Geology* **1992a**, *20*, 359–362.
(6) Hillner, P. E.; Manne, S.; Gratz, A. J.; Hansma, P. K. *Ultramicroscopy* **1992b**, *42−44*, 1387–1393.
(7) Britt, D. V.; Hlady, V. *Langmuir* **1997**, *13*, 1873–1876.
(8) Lea, A. S.; Amonette, J. E.; Baer, D. R.; Liang, Y.; Colton, N. G. *Geochim. Cosmochim. Acta* **2001**, *65*, 369–379.
(9) Usher, C. R.; Baltrusaitis, J.; Grassian, V. H. *Langmuir* **2007**, *23*, 7039–7045.
(10) de Leeuw, N. H.; Parker, S. C. *Langmuir* **1998**, *14*, 5900–5906.
(11) Cygan, R. T.; Wright, K.; Fisler, D. K.; Gale, J. D.; Slater, B. *Mol. Simul.* **2002**, *28*, 475–495.
(12) Kristensen, R.; Stipp, S. L. S.; Refson, K. *J. Chem. Phys.* **2004**, *121*, 8511–8523.
(13) Hay, M. B.; Workman, R. K.; Manne, S. *Langmuir* **2003**, *19*, 3727–3740.
(14) Godelitsas, A.; Astilleros, J. M.; Hallam, K.; Harissopoulos, S.; Putnis, A. *Environ. Sci. Technol.* **2003**, *37*, 3351–3360.
(15) Godelitsas, A.; Astilleros, J. M.; Hallam, K. R.; Löns, J.; Putnis, A. *Min. Mag.* **2003**, *67*, 1193–1204.
(16) Freij, S. J.; Putnis, A.; Astilleros, J. M. *J. Cryst. Growth* **2004**, *267*, 288–300.
(17) Freij, S. J.; Godelitsas, A.; Putnis, A. *J. Cryst. Growth* **2005**, *273*, 535–545.

(18) Astilleros, J. M.; Pina, C. M.; Fernández-Díaz, L.; Prieto, M.; Putnis, A. *Chem. Geol.* **2006**, *225*, 322–335.
(19) Vavouraki, A. I.; Putnis, C. V.; Putnis, A.; Koutsoukos, P. G. *Min. Mag.* **2008**, *72*, 145–148.
(20) Vavouraki, A. I.; Putnis, C. V.; Putnis, A.; Koutsoukos, P. G. *Chem. Geol.* **2008**, *253*, 243–241.
(21) Nygren, M. A.; Gay, D. H.; Catlow, R. A.; Wilson, M. P.; Rohl, A. L. *J. Chem. Soc., Faraday Trans.* **1998**, *94*, 3685–3693.
(22) de Leeuw, N. H. *J. Phys. Chem. B* **2002**, *106*, 5241–5249.
(23) Morse, J. W.; Arvidson, R. S.; Lüttge, A. *Chem. Rev.* **2007**, *107*, 342–381.
(24) de Leeuw, N. H.; Cooper, T. G. *Cryst. Growth Des.* **2004**, *4*, 123–133.
(25) Kim, W. I.; Darragh, M. R.; Orme, C.; Evans, J. S. *Cryst. Growth Des.* **2006**, *6*, 5–10.
(26) Kim, W. I.; Giocondi, J. L.; Orme, C.; Collino, S.; Evans, J. S. *Cryst. Growth Des.* **2008**, *8*, 1154–1160.
(27) Carpenter, R. *Geochim. Cosmochim. Acta* **1969**, *33*, 1153–1167.
(28) Ayoob, S.; Gupta, A. K. *Crit. Rev. Environ. Sci. Technol.* **2006**, *36*, 433–487.
(29) Senior, L. A.; Sloto, R. A. *U.S. Geol. Surv. Sci. Invest. Rep.* **2006**, *5261*, 1–105.
(30) Skinner, H. C. W. *Annu. Rev. Earth Planet. Sci.* **2007**, *35*, 177–213.
(31) Coggon, D.; Cooper, C. *Br. Med. J.* **1999**, *319*, 269–270.
(32) Sujana, M. G.; Pradhan, H. K.; Anand, A. *J. Hazard. Mater.* **2008**, *161*, 120–125.
(33) Fan, X.; Parker, D. J.; Smith, M. D. *Water Res.* **2003**, *37*, 4929–4937.
(34) Pommerenk, P.; Schafran, G. C. *Environ. Sci. Technol.* **2005**, *39*, 6429–6434.
(35) Turner, B.; Binning, P.; Stipp, S. L. S. *Environ. Sci. Technol.* **2005**, *39*, 9561–9568.
(36) Turner, B. D.; Binning, P. J.; Sloan, S. W. *J. Contam. Hydrol.* **2008**, *95*, 110–120.
(37) Kitano, Y.; Okumura, M. *Geochem. J.* **1973**, *7*, 37–49.
(38) Ohde, S.; Kitano, Y. *Geochem. J.* **1980**, *14*, 321–324.
(39) Okumura, M.; Kitano, Y.; Idogaki, M. *Geochem. J.* **1983**, *17*, 257–263.
(40) Parkhurst, D. L.; Appelo, C. A. J. *U.S. Geol. Survey Water-Resour. Invest. Rep.* **1999**, *99−4259*, 312.
(41) Plummer, N. L.; Busenberg, E. *Geochim. Cosmochim. Acta* **1982**, *46*, 1011–1040.
(42) Nordstrom, D. K.; Plummer, L. N.; Langmuir, D.; Busenberg, E.; May, H. M.; Jones, B. F.; Parkhurst, D. L. In Melchior, D. C.; Basset, R. L., Eds.; *Chemical Modeling of Aqueous Systems II*; American Chemical Society: Washington, DC, 1990; pp 398−413.
(43) Teng, H. H.; Dove, P. M.; Orme, C. A.; De Yoreo, J. J. *Science* **1998**, *282*, 724–727.
(44) Chernov, A. A.; Petrova, E. V.; Rashkovich, L. N. *J. Cryst. Growth* **2006**, *289*, 245–254.
(45) Nehrke, G.; Reichart, G. J.; Van Cappellen, P.; Meile, C.; Bijma, J. *Geochim. Cosmochim. Acta* **2007**, *71*, 2240–2249.
(46) Zhang, J.; Nancollas, G. H. *J. Colloid Interface Sci.* **1998**, *200*, 131–145.
(47) Pérez-Garrido, C.; Fernández-Díaz, L.; Pina, C. M.; Prieto, M. *Surf. Sci.* **2007**, *601*, 5499–5509.
(48) Teng, H. H.; Dove, P. M.; De Yoreo, J. J. *Geochim. Cosmochim. Acta* **2000**, *64*, 2255–2266.
(49) Stipp, S. L. S.; Eggleston, C. M.; Nielsen, B. S. *Geochim. Cosmochim. Acta* **1994**, *58*, 3023–3033.
(50) Teng, H. H.; Dove, P. M.; De Yoreo, J. J. *Geochim. Cosmochim. Acta* **1999**, *63*, 2507–2512.
(51) Astilleros, J. M.; Pina, C. M.; Fernández-Díaz, L.; Putnis, A. *Chem. Geol.* **2003**, *193*, 93–107.
(52) Liang, Y.; Baer, D. R. *Surf. Sci.* **1997**, *373*, 275–287.
(53) Sangwal, K. *North-Holland Phys.* **1987**, *15*, 497.
(54) Staudt, W. J.; Reeder, R. J.; Schoonen, M. A. A. *Geochim. Cosmochim. Acta* **1994**, *58*, 2087–2098.
(55) Paquette, J.; Reeder, R. J. *Geochim. Cosmochim. Acta* **1995**, *59*, 735–749.
(56) Shiraki, R.; Rock, P. A.; Casey, W. H. *Aq. Geochem.* **2000**, *6*, 87–108.
(57) Liang, Y.; Lea, A. S.; Baer, D. R.; Engelhard, M. H. *Surf. Sci.* **1996**, *351*, 172–182.
(58) Park, N. S.; Kim, M. W.; Langford, S. C.; Dickinson, J. T. *Langmuir* **1996**, *12*, 4599–4604.
(59) De Giudici, G. *Am. Mineral.* **2002**, *87*, 1279–1285.
(60) Davis, K. J.; Dove, P. M.; Wasylenki, L. E.; De Yoreo, J. J. *Am. Mineral.* **2004**, *89*, 714–720.
(61) Chernov, A. A. *Contemp. Phys.* **1989**, *30*, 251–276.
(62) Prieto, M.; Fernández-González, A.; Putnis, A.; Fernández-Díaz, L. *Geochim. Cosmochim. Acta* **1997**, *61*, 3383–3397.
(63) van Enckevort, W. J. P.; van den Berg, A. C. J. F. *J. Cryst. Growth* **1998**, *183*, 441–455.
(64) Sangwal, K. *Progr. Cryst. Growth Charact. Mater.* **1996**, *32*, 3–43.
(65) Astilleros, J. M.; Pina, C. M.; Fernández-Díaz, L.; Putnis, A. *Geochim. Cosmochim. Acta* **2000**, *64*, 2965–2972.
(66) Astilleros, J. M.; Pina, C. M.; Fernández-Díaz, L.; Putnis, A. *Geochim. Cosmochim. Acta* **2002**, *66*, 3177–3189.
(67) Davis, K. J.; Dove, P. M.; De Yoreo, J. J. *Sci. Mag.* **2000**, *290*, 1134–1137.
(68) Wasylenki, L. E.; Dove, P. M.; Wilson, D. S.; De Yoreo, J. J. *Geochim. Cosmochim. Acta* **2005**, *69*, 3017–3027.
(69) Teng, H. H.; Dove, P. M. *Am. Mineral.* **1997**, *82*, 878–887.
(70) Chernov, A. A. *Soviet Phys.* **1961**, *4*, 116–148.
(71) Astilleros, J. M.; Pina, C. M.; Fernández-Díaz, L.; Putnis, A. *Geochim. Cosmochim. Acta* **2003**, *67*, 1601–1608.
(72) Prieto, M.; Astilleros, J. M.; Pina, C. M.; Fernández-Díaz, L.; Putnis, A. *Am. J. Sci.* **2007**, *307*, 1034–1045.
(73) Cabrera, N.; Vermilyea, D. A. *Growth and Perfection of Crystals;* John Wiley & Sons Inc.: New York, 1958; p 393.
(74) Gratz, J. A.; Hiliner, P. E. *J. Cryst. Growth* **1993**, *129*, 789–793.
(75) Dove, P. M.; Hochella, M. F., Jr. *Geochim. Cosmochim. Acta* **1993**, *57*, 705–714.
(76) Dove, P. M.; Han, N.; De Yoreo, J. D. *Proc. Nat. Acad. Sci.* **2005**, *102*, 15357–15362.
(77) Glover, E. D.; Sippel, R. F. *Am. Mineral.* **1962**, *47*, 1156–1165.
(78) Harstad, A. O.; Stipp, S. L. S. *Geochim. Cosmochim. Acta* **2007**, *71*, 56–70.
(79) Hong, Q.; Surez, M. F.; Coles, B. A.; Compton, R. G. *J. Phys. Chem. B* **1997**, *101*, 5557–5564.
(80) Møller, H.; Lundager Madsen, H. E. *J. Cryst. Growth* **1985**, *71*, 673–681.
(81) Becker, U.; Biswas, S.; Kendall, T.; Risthaus, P.; Putnis, C. V.; Pina, C. M. *Am. J. Sci.* **2005**, *305*, 791–825.
(82) Piana, S.; Jones, F.; Gale, J. D. *J. Am. Chem. Soc.* **2006**, *128*, 13568–13574.
(83) Kowacz, M.; Putnis, C. V.; Putnis, A. *Geochim. Cosmochim. Acta* **2007**, *71*, 5168–5179.
(84) Kowacz, M.; Putnis, A. *Geochim. Cosmochim. Acta* **2008**, *72*, 4476–4487.
(85) Stipp, S. L. S.; Konnerup-Madsen, J.; Franzreb, K.; Kulik, A.; Mathieu, H. J. *Nature* **1998**, *396*, 356–359.
(86) Lakshtanov, L. Z.; Stipp, S. L. S. *Geochim. Cosmochim. Acta* **2004**, *68*, 819–827.
(87) Ishikawa, M.; Ichikuni, M. *Chem. Geol.* **1984**, *42*, 137–146.
(88) Busenberg, E.; Plummer, L. N. *Geochim. Cosmochim. Acta* **1985**, *49*, 713–725.